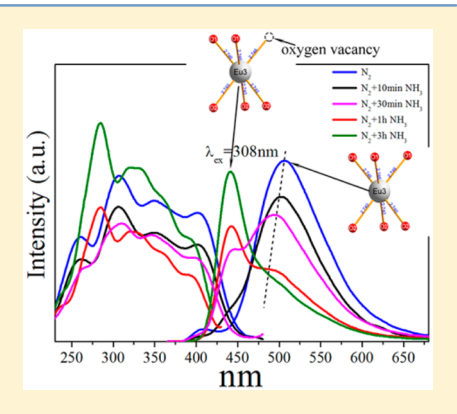
Inorganic Chemistry

Role of Oxygen Vacancy on the Photoluminescence of BaMgSiO₄:Eu Phosphors: Experimental and Theoretical Analysis

Weiwei Ji,[†] Ming-Hsien Lee,[‡] Luyuan Hao,[†] Xin Xu,*^{,†} Simeon Agathopoulos,[§] Dewen Zheng,^{||} and Chaohe Fang"

ABSTRACT: Pure BaMgSiO₄:Eu²⁺ phosphor, prepared by a solid state reaction method under N₂ atmosphere, exhibited a strong green emission at 500 nm and a weak emission at 405 nm. Heat treatment under NH3 atmosphere causes changes in the PL intensity: the green emission at 500 nm gradually decreases and completely disappears after heat treatment for 3 h, whereas a new blue emission peak, centered at 445 nm, appears and becomes very strong. The results of the analyses with electron paramagnetic resonance (EPR), X-ray photoelectron spectroscopy (XPS), and X-ray absorption fine structure (XAFS) spectroscopy suggest that the heat treatment causes the generation of a large amount of oxygen vacancies. This resulted in the aforementioned color changes of the BaMgSiO₄:Eu phosphor, which are confirmed by the results of DFT+U calculations. In particular, these calculations showed that Eu prefers to occupy Ba(3) sites, which are six coordinated to oxygen atoms. The emission at 500 nm was attributed to the 4f-5d transition energy of Eu in Ba(3) site, calculated as 2.54 eV. It was also shown that Eu 4f energy level decreases when



oxygen is removed from the oxygen position adjacent to Eu, which results in a larger Eu 4f-5d transition energy and shorter wavelengths of emission peaks.

■ INTRODUCTION

Alkaline earth silicates lend themselves as luminescent hosts because of their remarkable stability of physical and chemical properties, and crystalline structure, along with a relatively easy preparation process. 1-4 In particular, Eu²⁺-activated binary and ternary silicates attract special interest due to their photoluminescence properties. 1,3,5,6

There are numerous applications for BaMg-SiO₄:Eu²⁺compounds, such as white LEDs,⁸ long-persisting phosphors,⁹ and light photochromism.^{10–12} Blasse et al.¹³ and Poort et al.² have reported that the maximum emission of Eu²⁺ in Ba(3) sites (which are six coordinated to oxygen atoms) in BaMgSiO₄:Eu²⁺ occurs at 440 nm, and the emission bands of Eu^{2+} in Ba(1) and Ba(2) sites are at 510 and 570 nm, at 4.2 K. The latter two emission bands are almost quenched at room temperature.² Peng et al.¹⁴ and Li et al.⁹ have reported that BaMgSiO₄:Eu²⁺compounds have two emission peaks at 405 nm, due to Eu²⁺ in Ba(3) sites, and 500 nm due to Eu²⁺ in Ba(1) and Ba(2) sites, which are attributed to the preferential orientation of a d orbital of Eu²⁺ ion.^{2,15} This assignment apparently opposes the crystal field theory, where Eu²⁺ in a Ba(3) site should exhibit a longer emission wavelength due to the shorter average distance of Ba-O. Therefore, detailed

investigations on the photoluminescence properties of BaMgSiO₄:Eu²⁺ phosphors are required.

In this work, we synthesized BaMgSiO₄ doped with Eu²⁺ through solid state reaction, which exhibits a strong green emission at 500 nm and a weak emission at 405 nm. We found for the first time that the PL intensity of the green emission at 500 nm gradually decreases and completely disappears with heat treatment for 3 h, whereas a new blue emission peak, centered at 445 nm, appears. Thus, the working hypothesis aims at the cause of the change of the emission spectra, which is proposed to occur because of the generation of an oxygen vacancy on the adjacent site to Eu doped in BaMgSiO₄. Electron paramagnetic resonance (EPR), X-ray photoelectron spectroscopy (XPS), and X-ray absorption fine structure (XAFS) techniques were employed. Density functional theory (DFT) is an efficient method for studying optical properties of luminescent materials.^{7,16,17} Thus, we performed the DFT + U calculations to obtain the electronic structure of BaMg-SiO₄:Eu²⁺ with and without oxygen vacancies. The calculating results shed light on the cause of the aforementioned photoluminescence properties.

Received: October 23, 2014 Published: February 2, 2015

1556

[†]Chinese Academy of Sciences Key Laboratory of Materials for Energy Conversion, Department of Materials Science and Engineering, University of Science and Technology of China, Jinzhai Road 96, Hefei Anhui 230026, People's Republic of China

[‡]Department of Physics, Tamkang University, New Taipei City 25137, Taiwan

[§]Materials Science and Engineering Department, University of Ioannina, GR-451 10 Ioannina, Greece

Research Institute of Petroleum Exploration and Development-LangFang, Langfang Hebei 065000, People's Republic of China

■ EXPERIMENTAL SECTION

The phosphors were produced with a solid state reaction method, where $BaMgSiO_4$ was doped with 0.01 mol Eu^{2+} . Stoichiometric amounts of fine powders of $BaCO_3$ (99.99%), MgO (99.99%), SiO_2 (99.99%), and Eu_2O_3 (99.99%) were mixed with absolute ethanol and then milled using a planetary ball mill for 24 h to obtain a homogeneous mixture. The mixture was placed in alumina crucibles and then fired at 1400 °C for 6 h under flowing N_2 (1 atm). The assynthesized $BaMgSiO_4:Eu^{2+}$ powder (denoted as N_2) was subjected to a heat treatment under flowing NH_3 at 1150 °C for different times, specifically 10 min (denoted as N_2+10 min NH_3), 30 min (N_2+30 min NH_3), 1 h (N_2+1 h NH_3), and 3 h (N_2+3 h NH_3). For comparison purposes, the reduction of the as-synthesized phosphors was also attempted using H_2 gas.

The crystalline phases were identified with X-ray diffraction analysis (XRD, Philips PW 1700) using Cu Kα1 radiation at a scanning rate of 0.5°/min. The emission and excitation spectra were measured at room temperature with a fluorescent spectrophotometer (F-4600, Hitachi, Japan) with a 200 W Xe-lamp as an excitation source. The emission spectrum was corrected for the spectral response of a monochromator and Hamamatsu R928P photomultiplier tube (Hamamatsu Photonics K.K., Hamamatsu, Japan) by a light diffuser and tungsten lamp (Noma Electric Corp., NY; 10 V, 4A). The excitation spectrum was also corrected for the spectral distribution of the xenon lamp intensity by measuring rhodamine-B as a reference. Room-temperature EPR spectra were obtained on a JEOL JES-FA200 EPR. spectrometer (300 K, 9650 MHz, X band). X-ray photoelectron spectroscopy (XPS) was performed on an ESCALAB 250 X-ray photoelectron spectrometer with Al K α radiation. The decay time was recorded on a spectrophotometer (FLS920, Edinburgh Instruments Ltd.). The Xray absorption spectra at the Eu L3-edge were measured at the beamline of BL14W1 of the Shanghai Synchrotron Radiation Facility. The synchrotron ring was operated at 3.5 GeV at a 300 mA beam current with "top-up" mode. Energy resolution of the focused incoming X-rays was achieved using a Si(111) double-crystal monochromator. Fluorescence spectra were collected with a 32element Ge detector with accumulation time 3 s/5 s. An incident X-ray beam of 0.3 mm (H) \times 0.3 mm (V) dimensions (photon flux >1.0 \times 10¹³ phs/s) was used for the XANES experiments. All measurements were done at room temperature.

■ COMPUTATIONAL METHOD

Our calculations were based on density functional theory (DFT) within the generalized gradient approximation (GGA) proposed by Perdew, Burke, and Ernzerhof (PBE)¹⁸ using the CASTEP code. ^{19,20} The code used the iterative diagonalization technique to minimize the total energy with respect to the plane-wave coefficients. q_c -tuned optimized norm-conserving pseudopotentials³⁶ were generated using OPIUM code,³⁷ and GGA-PBE exchange-correlation functional was used to generate these pseudopotentials in order to be consistent with the later solid state electronic structure calculations. Except for the first row element oxygen, shallow core levels of elements (namely 2s, 2p for Mg and 5s, 5p for Ba and Eu) have all been treated as valence to increase the accuracy and transferability of pseudoptentials. Extensive tests have been performed on these pseudopotentials, and special attention has been paid to the fine-tuning of Eu pseudopotential. It reproduced reasonable lattice parameter for metallic Eu and oxide EuO, and the band structure also agreed well with published results. With the above-mentioned accurate pseudopotentials including rare-earth, 900 eV plane-wave energy was used to achieve total energy convergence to be within 0.1 eV per atom. Here, 84-atoms (i.e., 1 hexagonal supercell BaMgSiO₄:Eu) and 83-atoms (i.e., 1 hexagonal supercell BaMgSiO₄:Eu with an oxygen vacancy) were used in the calculations. The k-point samplings for the supercells were 3×3 × 1, according to the Monkhorst-Pack scheme, 21 which generates 10 and 18 irreducible k-points, respectively, in the irreducible Brillouin zone (BZ). The parameters for convergence control of the geometry optimization were 1×10^{-5} eV/atom for total energy, 0.03 eV/Å for maximum force, 0.05 GPa for stress, and 0.001 Å for displacement.

The SCF energy convergence threshold was set as $1\times 10^{-6}~\rm eV/atom$ to ensure the accuracy of the electronic calculation. The electronic correlation associated with the forbitals of Eu was treated in a mean field approach by adding an effective Hubbard on-site repulsion $U_{\rm eff}=3~\rm eV$ on Eu. This GGA + U treatment was necessary to properly describe absorption edge of rare earth contained materials. It should be noted that our calculation results is not sensitive to $U_{\rm eff}$.

In our calculations, we first carried out full geometry relaxations for the model compounds $BaMgSiO_4{:}Eu$ (E-BMS) and $BaMgSiO_4{:}Eu$ with an oxygen vacancy (E-BMS- $\!V_O\!$). Then, we calculated the single-point energy, density of state, and band structure of E-BMS and E-BMS- $\!V_O\!$.

Figure 1 shows the structure of BMS. There are three different barium sites that occur in equal amounts in the lattice.²² The sites of

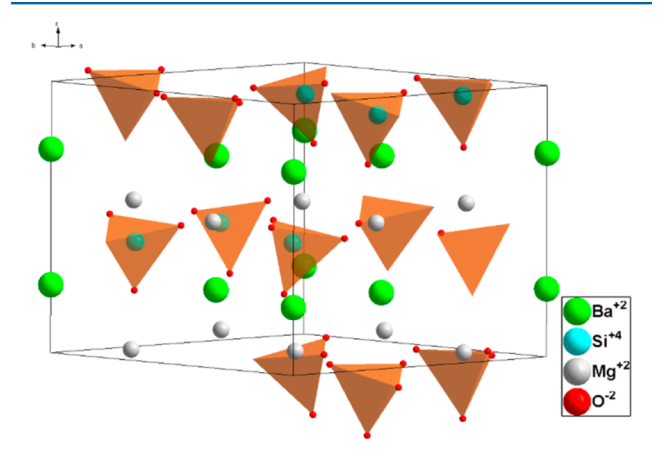


Figure 1. Crystal structure of BaMgSiO₄, where Ba²⁺ is green, Mg²⁺ is gray, O^{2-} is red located at the corners of the tetrahedra, and Si⁴⁺ is inside the tetrahedra with light blue color.

Ba(1) and Ba(2) are coordinated to nine oxygen ions with average Ba-O distances of 2.89 Å for Ba(1) and 2.94 Å for Ba(2). The third barium site, Ba(3), is coordinated to six oxygen ions with a shorter average Ba-O distance of 2.74 Å.

Figure 2 shows the coordination of Eu when it is doped in $BaMgSiO_4$. When Eu substitutes barium in Ba(1) or Ba(2) sites, it has

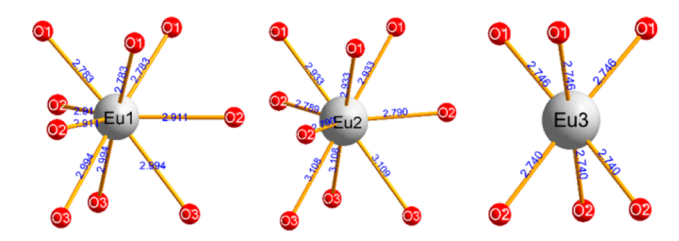


Figure 2. Coordination of Eu doped in BaMgSiO₄.

three kinds of coordinated oxygen anions, while in the Ba(3) site, it has two kind of oxygen anions. Accordingly, we built models of BaMgSiO₄ with the Ba(1) site replaced with Eu (BMS:Eu1) and BMS:Eu1 with an oxygen vacancy nearby (BMS:Eu1-V_{O1}, BMS:Eu1-V_{O2}, BMS:Eu1-V_{O3}). Similarly, other models, like BMS:Eu2, BMS:Eu2-V_{O1}, BMS:Eu2-V_{O2}, BMS:Eu2-V_{O3}, BMS:Eu3, BMS:Eu3-V_{O1}, and BMS:Eu3-V_{O2}, were also established.

RESULTS AND DISCUSSION

Figure 3 shows the diffractograms of the $BaMgSiO_4$:Eu phosphors as-synthesized in N_2 atmosphere and after postreduction in NH_3 atmosphere for different times. All of the recorded peaks can be assigned to the phase of $BaMgSiO_4$ (hexagonal, space group of $P6_322$, JCPDS card 81-2317),

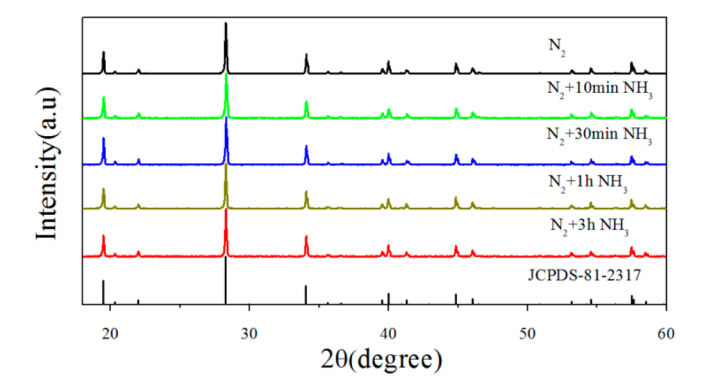


Figure 3. X-ray diffractograms of the BaMgSiO₄:Eu phosphor powders as-synthesized in N2 atmosphere and after postreduction in NH3 atmosphere for different times.

suggesting high purity and crystallinity of the produced powders. There is no evidence of phase transformation or the presence of secondary or impurity phases, even after 3 h of reduction.

The unit cell constants have also been calculated using the Jade 5.0 program. No obvious changes have been detected for the as-prepared (i.e., in N_2) sample (a = b = 9.1260 Å, c =8.7372 Å) and the sample postreduced in NH₃ atmosphere for 3 h (a = b = 9.1257 Å, c = 8.7370 Å). This indicates that the appearance of oxygen vacancies has little influence on the unit cell parameters.

Figure 4 shows the excitation and emission spectra of these BaMgSiO₄:Eu phosphors as-synthesized in N₂ atmosphere and

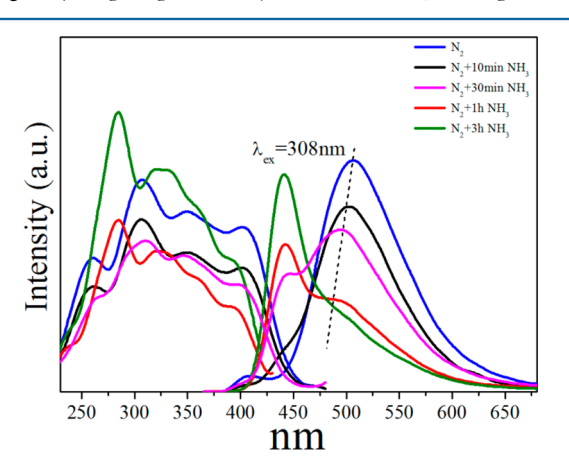


Figure 4. Excitation and emission spectra of the BaMgSiO₄:Eu phosphor powders as-synthesized in N2 atmosphere and after heat treatment in NH3 atmosphere for different times.

after heat treatment in NH₃ atmosphere for different times. It is clearly seen that the as-prepared (i.e., in N₂) phosphor has two emission peaks at 405 and 500 nm. This spectrum features remarkable differences from those reported by Poort et al.² and Blasse et al., ¹³ but is similar to those reported by Sivakumar et al., ⁸ Li et al., ⁹ and Peng et al. ¹⁴ In refs 8, 9, and 14, the emission peak at 405 nm was assigned to Eu²⁺ ions in Ba(3) sites, and the emission peak at 500 nm was assigned to Eu²⁺ ions in Ba(1) and Ba(2) sites.

As reported previously, Eu²⁺ with a higher coordination number generally emits at higher energy than that with a lower coordination number. 40,41 However, for the same coordination number, crystal field splitting (D_q) of Eu^{2+} 5d orbital can be determined by the following equation: 42,43

$$D_{q} = \frac{1}{6} Z e^{2} \frac{r^{4}}{R^{5}} \tag{1}$$

Here, D_a is a measure of the energy level separation, Z is the anion charge, e is the electron charge, r is the radius of the d wave function, and R is the bond length. High crystal field splitting leads to a red-shift of 5d-4f transition of Eu²⁺. These mean that Eu(3) with a lower coordination number and a smaller Eu-O distance (R) should exhibit longer wavelength emission. Although this conclusion apparently marks a difference between this work and earlier publications, it agrees fairly well with our calculated results, which are shown later in this Article.

With regard to the influence of the heat treatment with NH₃ on the luminescence of the produced phosphors, Figure 4 shows that the emission peak at 500 nm slightly blue-shifts and weakens, and eventually disappears in the samples produced after a prolonged (3 h) heat treatment in NH3. At the same time, a newly formed peak at 445 nm is recorded, and its intensity gradually increases with a longer heat treatment with NH₃. The peak at 405 nm also disappears gradually together with the peak at 500 nm.

We suggest that the slight blue-shift and the disappearance of the emission peak at 500 nm along with the appearance of the emission peak at 445 nm are due to oxygen vacancies generated by the heat treatment. To shed light on whether this suggestion can be further considered or if the above findings are due to nitrogen doping, BaMgSiO₄:Eu was also heat-treated in a 5% H₂ + 95% Ar atmosphere under the same experimental conditions. Similar tendencies of blue-shift were found. Thus, the effect of nitrogen on the emission spectrum can be ignored.

The luminescent decay curves of the 445 and 500 nm emissions of these BaMgSiO4:Eu phosphors were also measured. All the decay curves can be fitted on the basis of the well-known one exponential function. The lifetimes of Eu monitored at 445 and 500 nm are shown in Table 1. The PL

Table 1. Lifetimes of Eu Emission Monitored at 445 and 500 nm in BaMgSiO₄:Eu Phosphor Powders As-Synthesized in N₂ Atmosphere and after Heat Treatment in NH₃ Atmosphere for Different Times

	lifetimes (μs)	
	445 nm	500 nm
N_2		0.58
$N_2 + 10 \min NH_3$	0.23	0.60
$N_2 + 30 \min NH_3$	0.26	0.58
$N_2 + 1 h NH_3$	0.25	0.59
$N_2 + 3 h NH_3$	0.26	

lifetimes of both emission wavelengths remain unchanged, indicating that the two emissions occur independently, and the concentration of oxygen vacancies has little influence on the lifetimes of both emission wavelengths.

The electron paramagnetic resonance (EPR) spectra for these BaMgSiO₄:Eu phosphors, as-synthesized in N₂ atmosphere and after heat treatment in NH3 atmosphere for 3 h, are shown in Figure 5. There is no evidence for an EPR signal for the BaMgSiO4:Eu phosphor synthesized in N2 atmosphere, whereas a very strong EPR signal was recorded at 327.6 mT in

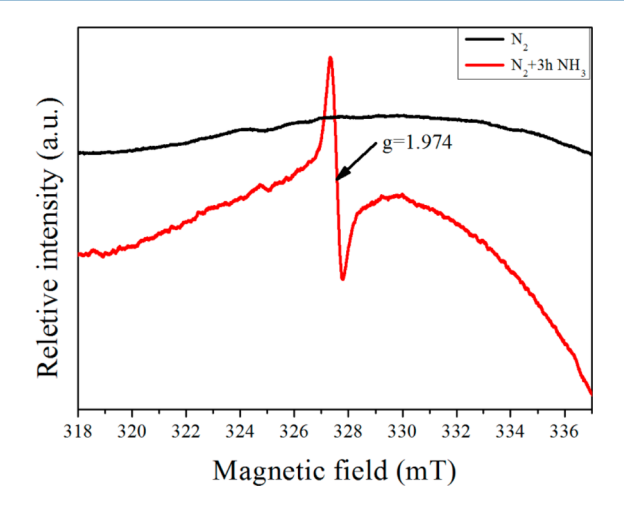


Figure 5. Electron paramagnetic resonance (EPR) spectra of the $BaMgSiO_4$:Eu phosphor powders as-synthesized in N_2 atmosphere and after heat treatment in NH_3 for 3 h.

the reduced phosphor. Yamaga et al.²³ reported a sharp signal at $g_z = 1.962$, $g_y = 1.958$, and $g_x = 1.960$ for the β -Ga₂O₃ crystal, assigned to O²⁻ vacancies trapping single electrons. Halliburton et al.²⁴ suggested that the symmetrical and sharp EPR signal at g = 1.96, detected in ZnO annealed in zinc vapor at 1100 °C for 30 min, is due to the electron trapped in the oxygen vacancy. Kumar et al.²⁵ have also observed a sharp EPR signal at g =2.002 and attributed this to an electron trapped in an oxygen vacancy. Matsuda et al. 26 detected two sharp EPR signals at g =1.939 and g = 2.003 in InGaZnO₄ and attributed them to the oxygen vacancy in different sites. This means that the oxygen vacancy with different cation coordination environments should result in different g-factors. According to the assignments given in the aforementioned earlier studies, the EPR signal at g =1.974 observed in the present study for the BaMgSiO₄:Eu phosphor heat-treated in NH3 atmosphere for 3 h can be assigned to an electron trapped in an oxygen vacancy.

The X-ray photoelectron spectroscopy (XPS) spectra of Ba 3d, Mg 2p, Si 2p, O 1s, and VBM (valence band maximum) of the BaMgSiO₄:Eu phosphor powders as-synthesized in the N₂ atmosphere and after heat treatment in NH₃ for 3 h are shown in Figure 6 (all spectra were calibrated with C 1s). It can be seen that the binding energy increases in Ba 3d, O 1s, and VBM, and decreases in Mg 2p and Si 2p after the heat treatment process.

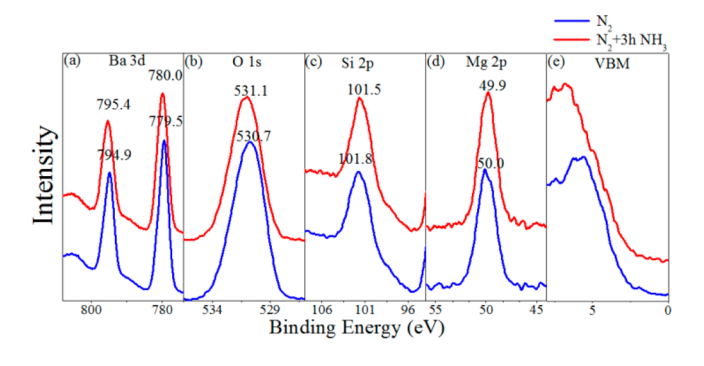


Figure 6. XPS spectra of (a) Ba 3d, (b) O 1s, (c) Si 2p, (d) Mg 2p, and (e) VBM (valence band maximum) of the BaMgSiO₄:Eu phosphor powders as-synthesized in N₂ atmosphere and after heat treatment in NH₃ for 3 h. All spectra were calibrated with C 1s peak.

The change of coordination environment in an atom causes a shift in the core level binding energy of the ion. 32,33 Tay et al. 27 have reported that oxygen vacancies close to the surface lead to the core level of O 1s and the valence band shifting to higher binding energies, which agrees well with our XPS results in O 1s and VBM. It was reported that the binding energy of barium is lowered by about 0.5 eV, with respect to metallic Ba upon oxidation. Setimer et al. have also reported that the Ba2+ site coordinated to more or less oxygen vacancies has higher Ba 3d binding energy compared to a Ba2+ site coordinated completely to O^{2-} ions. Müller et al. reported that oxygen-deficient MgO has a lower binding energy of Mg 2p than the subsequently oxidized MgO. Cho et al. have reported that the Si 2p binding energy shifts from 103 eV (\sim Si4+) to a low energy direction when oxygen is extracted from SiO2.

The variation of binding energy with heat treatment process suggests that oxygen vacancies form during the heat treatment in NH₃. Since this heat treatment process had a significant impact on the emission spectra, we suggest that oxygen vacancies should be generated close (i.e., adjacently) to the Eu in BMS:Eu during the heat treatment process.

Figure 7 shows the normalized Eu LIII-edge XANES of the BaMgSiO₄:Eu phosphor powders as-synthesized in N₂

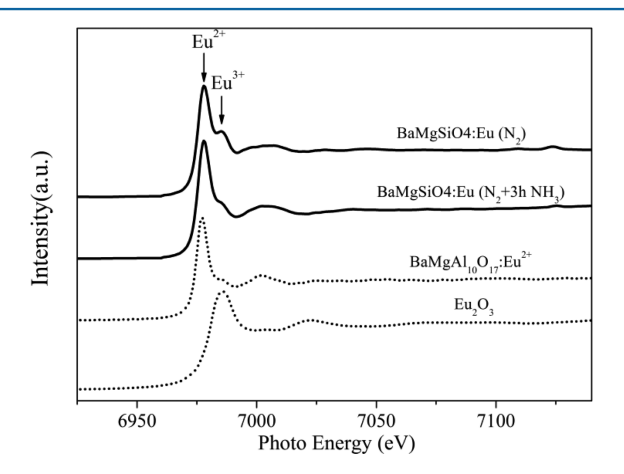


Figure 7. Normalized Eu LIII-edge XANES of the BMS:Eu phosphor powders as-synthesized in N_2 atmosphere and after heat treatment in NH $_3$ for 3 h. Dot curves represent the typical XANES spectra of divalent europium (BaMgAl $_{10}$ O $_{17}$:Eu $^{2+}$) and trivalent europium (Eu $_2$ O $_3$).

atmosphere and after heat treatment in NH $_3$ for 3 h. Two peaks can be clearly seen, at about 6977 and 6984 eV, which are due to the divalent and trivalent oxidation states of Eu, respectively. ^{32,33} It is clearly seen that the peak due to Eu³⁺ recorded in the as-synthesized BMS:Eu almost disappears after heat treatment in NH $_3$ for 3 h. We suggest that the oxygen vacancy, which forms adjacently to the Eu³⁺ during the heat treatment process, causes the reduction of Eu³⁺ to Eu²⁺. In particular, the oxygen vacancy (V_O*) formed during the reduction process acts as a donor and becomes a single charged oxygen vacancy (V_O*) (this was found in the EPR and XPS), and releases an electron. The Eu_{Ba}* becomes the acceptor of the electron and reduces Eu³⁺ to Eu²⁺. The formation of the oxygen vacancy adjacently to the Eu³⁺ during the heat treatment process that causes the reduction of Eu³⁺ to Eu²⁺ can be summarized in the following equation:

$$O_O^x + Eu_{Ba}^{\bullet} \xrightarrow{\text{heat in NH}_3} V_O^{\bullet} + \frac{1}{2}O_2 + Eu_{Ba}^X$$
 (2)

Figure 8 presents the band structures and density of state (DOS) of BMS:Eu3. The results reveal that BMS has a band

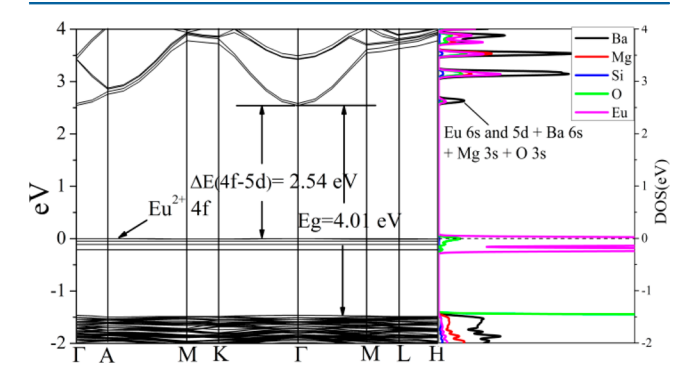


Figure 8. Band structures and DOS of BMS:Eu3 (Fermi surface is set to zero).

gap of ~4 eV, which agrees well with the absorption edge (280 nm) of the BMS without Eu²⁺ doping. Figure 9 shows the

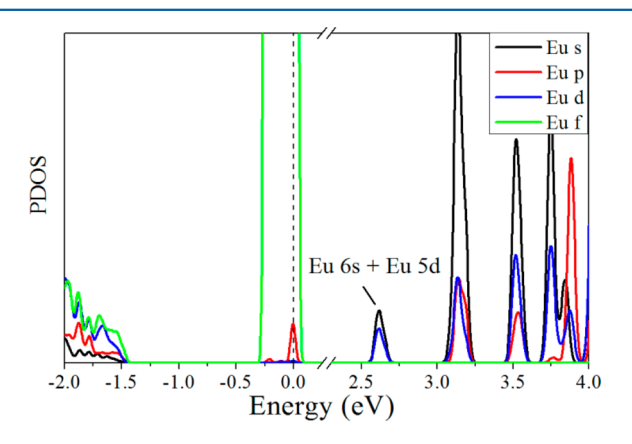


Figure 9. PDOS (partial density of states) of Eu in BMS:Eu3 from -2to 4 eV.

atom-resolved partial DOS (PDOS) for Eu in BMS:Eu3. The Eu 4f energy levels emerge on the Fermi surface and the majority spin states (spin \(\frac{1}{2}\)) of Eu 4f are fully occupied (which is also confirmed by Figure 12a, as shown later). The peak of the Eu 5d and Eu 6s states appears at 2.54 eV above the Fermi level (Figure 9). Unlike the localized Eu 4f orbitals illustrated, the Eu 5d orbitals expand in the entire conduction band and hybridize with Eu 6s, Ba 6s, Mg 3s, and O 3s states at the bottom of conduction band, as shown in Figures 8 and 9. The state of Eu 6s is stronger than that of Eu 5d at the bottom of the conduction band (Figure 9). However, the optical transition between the Eu²⁺ ion ground state of 4f and 6s is forbidden. Hence, we consider that the lowest energy transition mainly occurs between the Eu²⁺ 4f and 5d at the bottom of the conduction band.

The band structure and density of states of BMS-Eu1 and BMS-Eu2 are similar to that of BMS-Eu3.

Table 2 shows the Eu 4f-5d transition energy and relative total energy of Eu in different sites of BMS. It can be observed that BMS-Eu3 has a Eu 4f-5d transition energy of 2.54 eV, which is very close to the emission wavelength of 500 nm (2.48 eV). BMS-Eu1 and BMS-Eu2 have Eu 4f-5d transition

Table 2. Eu 4f-5d Transition Energy and Relative Total Energy of Eu in Different Sites of BMS

	transition energy (eV)	relative total energy (meV)
BMS:Eu1	2.90	0
BMS:Eu2	2.80	-85
BMS:Eu3	2.54	-219

energies of 2.80 and 2.90 eV, respectively, which are close to the emission wavelength of 405 nm (3.06 eV). Accordingly, we ascribe the emission peak at 500 nm to the Eu in Ba(3) sites and that at 405 nm to the Eu in Ba(1) and Ba(2) sites. These suggestions are also supported by the values of the relative total energy of Eu in different Ba sites of BMS. The relative total energy of BMS-Eu increases in the order BMS-Eu1, BMS-Eu2, and BMS-Eu3. Accordingly, Eu2+ should be strongly prone to being located at the Ba(3) site, which may explain why the emission peak at 500 nm is much stronger than that at 405 nm.

Figure 10 shows the band structure and DOS of BMS:Eu3- V_{O1} . Figure 11 shows the related atom-resolved partial DOS

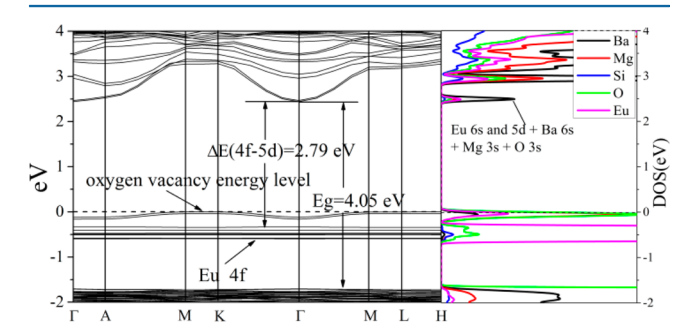


Figure 10. Band structure and DOS of BMS:Eu3-V_{O1}. The Fermi level is at 0 eV.

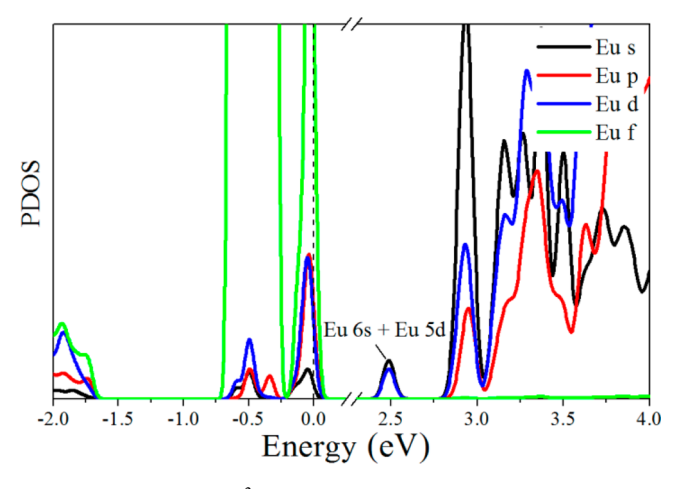


Figure 11. PDOS of Eu²⁺ in BMS:Eu3-V_{O1}.

(PDOS) for Eu. When an oxygen is removed from the O1 site of BMS:Eu3, oxygen vacancy defect energy levels emerge on the Fermi surface, which can be confirmed by Figure 12b. Eu localized 4f state moves down to ca. -0.35 eV. Note that the Eu 5d and 6s states in PDOS of Eu are mainly at the bottom of the conduction band, located at ~2.4 eV; thus, the lowest energy transition mainly occurs between the Eu²⁺ 4f and 5d states.

Figure 12 shows the orbital structures of BMS:Eu3 from -0.2 to 0 eV and BMS:Eu3-V_{O1} from -0.14 to 0 eV. The -0.2

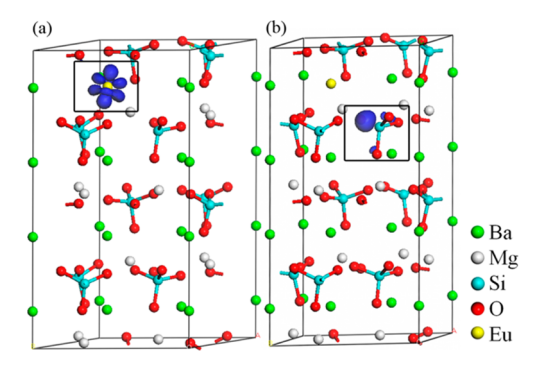


Figure 12. Orbital structures of (a) BMS:Eu3 -0.2 to 0 eV, and (b) BMS:Eu3-V_{O1} -0.14 to 0 eV. The blue translucent isosurfaces in the black frame represent the Eu majority 4f orbital in part a and the orbital of oxygen vacancy defect in part b.

to 0 eV orbital structure in Figure 12a is that for Eu 4f orbitals because the isosurfaces are localized on Eu and its nodal structure agrees well with the characteristic of an f orbital. The -0.14 to 0 eV orbitals in Figure 12b are localized around the O1 site, which is removed from BMS:Eu3. This indicates that the energy levels emerging on the Fermi surface are oxygen vacancy defect energy levels.

The band structure and density of states of BMS:Eu1- V_{O1} , BMS:Eu1- V_{O2} , BMS:Eu1- V_{O3} , BMS:Eu2- V_{O2} , BMS:Eu2- V_{O3} , and BMS:Eu3- V_{O2} are similar to that of BMS:Eu3- V_{O1} .

Table 3 shows the values of Eu 4f-5d transition energy and relative total energy of BMS:Eu, BMS:Eu-V_O, and the increase

Table 3. Eu 4f–5d Transition Energy and Relative Total Energy of BMS:Eu, BMS:Eu- V_O , and the Increase of Transition Energy when an Oxygen Atom Is Removed from the Site Adjacent to Eu

	transition energy (eV)	increase of energy transition (eV)	relative total energy (meV)
BMS:Eu1	2.90		
BMS:Eu1- V _{O1}	3.04	0.14	-363
BMS:Eu1- V _{O2}	2.95	0.05	0
BMS:Eu1- V _{O3}	3.20	0.30	-232
BMS:Eu2	2.79		
BMS:Eu2- V _{O1}	2.89	0.10	-195
BMS:Eu2- V _{O2}	2.91	0.12	-258
BMS:Eu2- V _{O3}	2.79	0.00	0
BMS:Eu3	2.54		
BMS:Eu3- V _{O1}	2.79	0.25	-90
BMS:Eu3- V _{O2}	2.94	0.40	0

of transition energy when an oxygen atom is removed from the site adjacent to Eu. The total energy of BMS:Eu3- V_{O1} is lower than that of BMS:Eu3- V_{O2} , indicating that oxygen vacancies are strongly prone to appear on O1 sites during heat treatment in NH₃. The experimental results show that the emission peak of BaMgSiO₄:Eu changes from 500 nm (2.48 eV) to 445 nm (2.79 eV) during heat treatment in NH₃ atmosphere. The

experimental energy increase of 0.31 eV agrees with our calculated value of 0.25 eV in BMS:Eu 3 -V $_{01}$.

In the case of Eu1 and Eu2, BMS:Eu1-VO1 and BMS:Eu2-VO2 have the lowest total energy, which lead to the blue-shifts of 0.14 and 0.16 eV, respectively. Due to the large overlap of the 405 nm emission band and the excitation bands of the 500 nm emission (Figure 4) in conjunction with the lower possibility of Eu²⁺ ions occupying Ba(1) and Ba(2) sites, the emission peak of 405 nm is weak, even in the as-synthesized BMS:Eu. After the heat treatment process, oxygen vacancies appear in the sites adjacent to Eu, according to our calculations, which should increase the Eu 4f-5d transition energy and blueshift the 405 nm emission peak toward shorter wavelengths. In the same manner, a wider overlap between the excitation and the emission bands occurs and an increasing amount of energy of the blue-shifted 405 nm peak is transferred to the 445 nm peak, resulting in the gradual disappearance of the emission peak at 405 nm.

To further investigate the reason for the change of the emission peak, we compared the band structure of BMS:Eu3 (Figure 8) with that of BMS:Eu3- V_{O1} (Figure 10). When the oxygen of the O1 site is removed from BMS:Eu3, the band gap $(E_{\rm g})$ of the matrix slightly increases from 4.01 to 4.05 eV. This means that the electrons localized in the oxygen vacancy site (Figure 10) have a weak influence on the energy levels of the matrix and the Eu 5d (Eu 5d orbital hybridizes with the matrix orbitals). However, the localized electrons in the oxygen vacancy site have a strong influence on the Eu 4f orbital; thus, the Eu 4f–5d transition energy changes from 2.54 to 2.79 eV.

Moreover, the slight blue-shift of the 500 nm emission peak can be interpreted as follows: the electrons localized in the oxygen vacancy site might slightly increase the 4f–5d transition energy of Eu3 in the sites without oxygen vacancy coordination due to the slight increase of the band gap of the matrix.

CONCLUSIONS

Color turning of BaMgSiO₄:Eu (BMS:Eu) phosphors was achieved by heat treatment under NH3. The experimental results of EPR, XPS, and Eu LIII-edge XANES of the BMS:Eu suggest that oxygen vacancies emerge on the oxygen sites adjacent to Eu doped in BMS. DFT+U calculations found that Eu prefers to occupy the Ba(3) sites, which are six coordinated to oxygen atoms. Eu in Ba(3) site has a 4f-5d transition energy of 2.54 eV, which is ascribed to the emission peak at 500 nm observed experimentally. Eu in Ba(1) and Ba(2) sites have 4f-5d transition energy of 2.90, 2.80 eV, respectively, ascribed to the 405 nm emission peak. DFT+U calculations reveal that the localized electrons in oxygen vacancy cause changes in the wavelength of the emission spectrum of BMS:Eu because of the decrease in the Eu 4f energy level. The emission peak at 405 nm gradually disappears due to the increasing overlap between the excitation and emission bands over the increasing time of the heat treatment process.

AUTHOR INFORMATION

Corresponding Author

*E-mail: xuxin@ustc.edu.cn. Fax: +86-551-3601592. Phone: +86-551-3600824.

Notes

The authors declare no competing financial interest.

ACKNOWLEDGMENTS

This research was supported by the National Natural Science Foundation of China (No. 51072191, 11179037) and CAS Strategic Priority Research Program (XDB10030402). The authors thank BL14W1 beamline of Shanghai Synchrotron Radiation Facility for providing XAFS measurements. We also thank the Supercomputing Center of USTC for their support in performing parallel computations. M.-H.L. thanks NCHC for database response support and the Key Win Electronics Co. for equipment donation.

REFERENCES

- (1) Barry, T. L. J. Electrochem. Soc. 1968, 115, 1181-1184.
- (2) Poort, S. H. M.; Reijnhoudt, H. M.; van der Kuip, H. O. T.; Blasse, G. J. Alloys Compd. 1996, 241, 75–81.
- (3) Ju, L.-C.; Cai, C.; Zhu, Q.-Q.; Tang, J.-Y.; Hao, L.-Y.; Xu, X. J. Mater. Sci.: Mater. Electron. 2013, 24, 4516–4521.
- (4) Sohn, K.-S.; Cho, B.; Park, H. D. J. Am. Ceram. Soc. 1999, 82, 2779-2784.
- (5) Suehiro, T.; Hirosaki, N.; Xie, R.-J.; Mitomo, M. Chem. Mater. **2005**, 17, 308-314.
- (6) Gu, Y.-X.; Zhang, Q.-H.; Li, Y.-G.; Wang, H.-Z. J. Mater. Chem. 2010, 20, 6050-6056.
- (7) Terakura, K. Prog. Mater. Sci. 2007, 52, 388-400.
- (8) Sivakumar, V.; Varadaraju, U. J. Electrochem. Soc. 2007, 154, J167–J171.
- (9) Li, Y.; Wang, Y.; Gong, Y.; Xu, X.; Zhang, F. Acta Mater. 2011, 59, 3174–3183.
- (10) Akiyama, M. Appl. Phys. Lett. 2010, 97, 181905.
- (11) Akiyama, M.; Yamada, H.; Sakai, K. J. Ceram. Soc. Jpn. 2011, 119, 338-341.
- (12) Akiyama, M.; Yamada, H.; Sakai, K. J. Ceram. Soc. Jpn. 2011, 119, 105–109.
- (13) Blasse, G.; Wanmaker, W.; Tervrugt, J.; Bril, A. Philips Res. Rep. 1968, 23, 189–200.
- (14) Peng, M.; Pei, Z.; Hong, G.; Su, Q. J. Mater. Chem. 2003, 13, 1202–1205.
- (15) Poort, S. H. M.; Blokpoel, W. P.; Blasse, G. Chem. Mater. 1995, 7, 1547-1551.
- (16) Tang, J.-Y.; Chen, J.; Hao, L.-Y.; Xu, X.; Xie, W.; Li, Q. J. Lumin. 2011. 131. 1101–1106.
- (17) Tang, J.-Y.; Gao, J.-K.; Chen, J.-H.; Hao, L.-Y.; Xu, X.; Lee, M.-H. Comput. Mater. Sci. 2013, 79, 478–484.
- (18) Perdew, J. P.; Burke, K.; Ernzerhof, M. Phys. Rev. Lett. 1996, 77, 3865—3868
- (19) Segall, M.; Lindan, P. J.; Probert, M.; Pickard, C.; Hasnip, P.; Clark, S.; Payne, M. J. Phys.: Condens. Matter 2002, 14, 2717.
- (20) Clark, S. J.; Segall, M. D.; Pickard, C. J.; Hasnip, P. J.; Probert, M. I.; Refson, K.; Payne, M. C. Z. Kristallogr. 2005, 220, 567–570.
- (21) Monkhorst, H. J.; Pack, J. D. Phys. Rev. B 1976, 13, 5188-5192.
- (22) Liu, B.; Barbier, J. J. Solid State Chem. 1993, 102, 115–125.
- (23) Yamaga, M.; Villora, E.; Shimamura, K.; Ichinose, N.; Honda, M. *Phys. Rev. B* **2003**, *68*, 155207.
- (24) Halliburton, L. E.; Giles, N. C.; Garces, N. Y.; Luo, M.; Xu, C.; Bai, L.; Boatner, L. A. Appl. Phys. Lett. **2005**, 87, 172108.
- (25) Kumar, M.; Singh, V. N.; Singh, F.; Lakshmi, K. V.; Mehta, B. R.; Singh, J. P. *Appl. Phys. Lett.* **2008**, 92, 171907.
- (26) Matsuda, T.; Nishimoto, D.; Takahashi, K.; Kimura, M. *Jpn. J. Appl. Phys.* **2014**, *53*, 03CB03.
- (27) Tay, Y.-Y.; Tan, T.-T.; Liang, M.-H.; Boey, F.; Li, S. Phys. Chem. Chem. Phys. **2010**, 12, 6008–6013.
- (28) Wertheim, O. K. J. Electron Spectrosc. Relat. Phenom. 1984, 34, 309-312.
- (29) Steiner, P.; Kinsinger, V.; Sander, I.; Siegwart, B.; Hüfner, S.; Politis, C. Z. Phys. B: Condens. Matter 1987, 67, 19–23.
- (30) Müller, M.; Matthes, F.; Schneider, C. M. J. Appl. Phys. 2007, 101, 09G519.

(31) Cho, D.-Y.; Oh, S.-J.; Chang, Y. J.; Noh, T. W.; Jung, R.; Lee, J.-C. Appl. Phys. Lett. **2006**, 88, 193502.

- (32) Wang, Y.-F.; Xu, X.; Yin, L.-J.; Hao, L.-Y. J. Am. Ceram. Soc. 2010, 93, 1534–1536.
- (33) Kim, K.-B.; Kim, Y.-I.; Chun, H.-G.; Cho, T.-Y.; Jung, J.-S.; Kang, J.-G. Chem. Mater. 2002, 14, 5045-5052.
- (34) Lee M.-H. Ph.D. Thesis, The University of Cambridge, 1995.
- (35) Lee M.-H.; Lin J.-S.; Payne M. C.; Heine V.; Milman V.; Crampin S. Wk Newsletters 67 (February) Highlights, 2005.
- (36) Rappe, A. M.; Rabe, K. M.; Kaxiras, K.; Joannopoulos, J. D. *Phys. Rev. B* **1990**, *41*, 1227.
- (37) See http://opium.sourceforge.net/index.html for information about the Opium pseudopotential generation project.
- (38) Figure 2 from: Jiang, H.; Rinke, P.; Scheffler, M. Phys. Rev. B **2012**, 86, 125115.
- (39) One of the authors (M.-H.L.) created and tested the pseudopotentials used, which have been (or soon will be) included in CASTEP Materials Studio Pseudopotential Library, where further details of their generation parameters and test results can be found.
- (40) Van Uitert, L. J. Lumin. 1984, 29, 1-9.
- (41) Yu, J.-Y.; Hao, Z.-D.; Zhang, X.; Luo, Y.-S.; Zhang, J.-H. Chem. Commun. 2011, 47, 12376–12378.
- (42) Jang, H. S.; Im, W. B.; Lee, D. C.; Jeon, D. Y.; Kim, S. S. J. Lumin. 2007, 126, 371–377.
- (43) Shang, M.-M.; Li, C.-X.; Lin, J. Chem. Soc. Rev. 2014, 43, 1372-